Sustainable Energy & Fuels

Detailed Chemical Composition of an Oak Biocrude and Its Hydrotreated Product Determined by Positive Atmospheric Pressure Photoionization Fourier Transform Ion Cyclotron Resonance Mass Spectrometry

Journal:	*Sustainable Energy & Fuels*
Manuscript ID	SE-ART-09-2019-000837.R1
Article Type:	Paper
Date Submitted by the Author:	03-Feb-2020
Complete List of Authors:	Ware, Rebecca; Florida State University, Chemistry & Biochemistry Rodgers, Ryan; Florida State University, National High Magnetic Field Laboratory Marshall, Alan; Florida State University, Department of Chemistry Mante, Ofei; RTI International, Energy Technology Division Dayton, David; Research Triangle Institute, Energy Technology Division; Verrdier, Sylvain; Haldor Topsoe AS Gabrielsen, Jostein; Haldor Topsoe AS Rowland, Steven; National Renewable Energy Laboratory, National Bioenergy Center

SCHOLARONE™
Manuscripts

Please do not adjust margins

ARTICLE

Detailed Chemical Composition of an Oak Biocrude and Its Hydrotreated Product Determined by Positive Atmospheric Pressure Photoionization Fourier Transform Ion Cyclotron Resonance Mass Spectrometry

Received 00th May 2019
Accepted 00th ???2019

DOI: 10.1039/x0xx00000x

Rebecca L. Ware[a], Ryan P. Rodgers[b,c], Alan G. Marshall[a,b], Ofei D. Mante[d], David C. Dayton[d], Sylvain Verdier[e], Steven M. Rowland[b,c]

The chemical composition of biomass-derived pyrolysis oils renders them undesirable for replacement of or blending with crude oils. The undesirable constituents result mainly from high oxygen content after pyrolysis, making oxygen the target for removal during subsequent upgrading. Catalytic hydrotreatment is the most common method for oxygen removal and can be performed during or after pyrolysis. The efficient removal of oxygen depends on its interaction with the catalyst, and therefore depends on the chemical composition of the oxygen-containing compounds. Knowledge of the oxygen composition before and after hydrotreatment provides insight into the removal process and possible applications for the upgraded oil. Here, we characterize an oak biocrude and its hydrotreated product by positive atmospheric pressure photoionization Fourier transform ion cyclotron resonance mass spectrometry to establish compositional changes that occur during hydrotreatment. A silica gel fractionation was also applied to enable separate analysis of the saturated and aromatic hydrocarbons from the hydrotreated pyrolysis oil.

Introduction

The properties of lignocellulosic pyrolysis oil make it poorly suited for either replacement or blending into fossil liquid fuels, due, in large part, to the high concentration of oxygen-containing compounds found in bio-oils.[1] Removal of oxygen by catalytic hydrotreatment (HDT) is carried out by two main methods, catalytic cracking and catalytic hydroprocessing. Catalytic cracking employs catalysts at high temperature (~500 °C) without H_2 gas. The catalyzed reactions include C-C bond cleavage, dehydration, decorboxylation, and decarbonylation. Catalytic hydroprocessing is performed at moderate temperature (~300 °C) and high H_2 pressure (~70 bar) with a catalyst to remove oxygen as carbon dioxide, carbon monoxide, and water through decarboxylation, decarbonylation, hydrodeoxygenation (HDO), and dehydration. Both approaches aim to improve pyrolysis oil properties and produce hydrocarbon-rich oils applicable to blending with refined petroleum. Ideally, oxygen is removed while retaining carbon and hydrogen, but in reality, oxygen removal correlates with unwanted carbon loss and formation of aromatic species. Many of the challenges associated with HDT result from the undesirable properties of bio-crudes, and therefore require additional preprocessing. Among the many methods for pretreatment, only catalytic fast pyrolysis (CFP) will be discussed here.

Removal of oxygen from biomass through CFP has been shown to decrease the acidity and viscosity, increase the storage stability, and shift the chemical composition of the pyrolysis oil closer to that of petroleum.[2–5] The catalyst facilitates the removal of oxygen as water, carbon dioxide, and carbon monoxide through dehydration, decarboxylation, and decarbonylation. Dayton et al.[5] designed a catalytic biomass pyrolysis unit to optimize the catalysis and operating conditions for biomass pyrolysis. Their system is a continuously circulating single loop that allows for monitoring of catalyst-to-biomass ratio, residence time, temperature, and feedrate. Pyrolysis takes place in a mixing zone that consists of hot catalyst (600-700 °C) from the regenerator, solid biomass injected with a feedscrew, and N_2 as fluidization gas for a residence time of ~0.75 s; converting the solid biomass into gases, bio-crude, water, char, and ash. The solids (catalyst, char, and ash) are separated from the pyrolysis vapors and transferred to the regenerator where the combustion of char and ash heats and regenerates the catalyst for recirculation back into the mixing zone. Fresh catalyst can also be added into the regenerator if needed. Water is used to condense the product vapors through direct contact; noncondensable gases are burned, and the liquids are collected and allowed to separate into aqueous and organic phases. This method produced a biocrude from loblolly pine (organic phase) that was shown by gas chromatography-mass spectrometry (GC-MS) to contain ~20 wt% aromatics (of which 90% were phenolics), ~13 wt% aldehydes and ketones, ~11 wt% levoglucosan, and ~2 wt% acids. However, the

[a] a. Department of Chemistry and Biochemistry, 95 Chieftain Way, Florida State University, Tallahassee, FL 32306, USA
[b] b. Ion Cyclotron Resonance Program, National High Magnetic Field Laboratory, Florida State University, Tallahassee, FL 32310, USA
[c] c. Future Fuels Institute, Florida State University, Tallahassee, FL 32310, USA
[d] d. Energy Technology Division, RTI International, Research Triangle Park, North Carolina, USA
[e] e. Haldor Topsoe A/S, Haldor Topsøes Allé 1, DK-2800 Kgs, Lyngby, Denmark

Please do not adjust margins

authors' analysis was limited because only ~50 wt% of components seen by GC-MS were quantified, and only ~59% of the bio-crude carbon was accounted for. Thus a significant number of higher molecular weight and/or non-volatile components in the bio-crude require alternative methods of analysis; such as Fourier transform ion cyclotron resonance (FT-ICR) mass spectrometry (MS).[6–8] Major concerns associated with CFP include the formation of water through dehydration, and hydrogen deficiency resulting in coke, and catalyst deactivation requiring new or regenerated catalysts. Finally, because not all oxygenated species are removed during CFP, further deoxygenation is necessary.

Mante et al.[9] integrated CFP and HDT to produce a hydrocarbon-based bio-oil from loblolly pine sawdust. CFP oil produced by RTI International's catalytic biomass pyrolysis unit[5] is less acidic, relatively stable, and less oxygenated, enabling more efficient HDT without additional preprocessing. The HDT unit consists of five sections; the first of which is the biocrude feed system. Here, the biocrude is pumped from the feed tanks into the reactor with a diaphragm pump. The gas feed section provides hydrogen via a compressor into the reactor. The reactor section contains two down-flow fixed-bed reactors that enable single or double stage hydrotreating; however, only single-stage hydrotreatment was reported. A sulfide NiMo catalyst, with high HDO activity and moderate HDN and HDS activities, was used. The gas/liquid separator system consists of high- and low-pressure separators, a nitrogen stripper, an oil/water separator, and collection pots for liquid products. The final section contains six programmable sampling stations throughout the HDT unit. This HDT system produces biocrude with reduced oxygen, nitrogen, and sulfur while increasing the H/C ratio. It was found that the carbon content of the biocrude was retained in the HDT liquid; meaning that less carbon was lost to gas, aqueous phase, or coke. Also, the liquid yields for this method were higher than previous HDT efforts.[10–17] GC with flame ionization detection (FID) of the liquid products yielded carbon numbers up to 23, thereby rendering the HDT liquids compatible with GC-MS for compound class identification. The oxygenates in the HDT liquid were mainly monofunctional, indicating that deoxygenation occurs by demethoxylation and dehydration. The catalyst and process conditions evidently favored a direct deoxygenation mechanism over hydrogenation based on the presence of simple phenols, aromatics, anisoles, and cyclic olefins.

HDT liquid products are accessible by GC because of their higher volatility and lower carbon number than biocrude. However, GC is not applicable for analysis of the biocrude and in turn not applicable for comparing biocrude and its upgraded counterpart. Negative-ion electrospray ionization ((-)ESI) and positive-ion atomspheric pressure photoionizaztion ((+)APPI) are the most common ionization techniques for biocrude FT-ICR MS.[7,18–22] Hertzog et al.[22] compared various ionization techniques for an oak-derived biocrude, and found that although there were differences in the observed ion compositions, the most abundant oxygen-containing heteroatom class distributions were similar. Derivatives of pyrolytic lignin and sugars were observed. The authors also reported carbon numbers up to 40 for the APPI mass spectra. McClelland et al.[7] analyzed an oak lignin pyrolysis oil and its hydrogenated counterpart by APPI FT-ICR MS. They found that hydrogenation resulted in a shift to slightly lower carbon number (maximum of 55 vs 50) and decrease in double bond equivalents (DBE = number of rings and double bonds to carbon) (maximum 35 vs 25), as well as similar shifts for the oxygen-containing species. Here, we analyze an oak biocrude and its upgraded product produced by the CFP and subsequent HDT discussed above. Samples were fractionated on silica gel and analyzed by (+)APPI FT-ICR MS.

Experimental Methods

Feedstock. Red oak was received from Iowa State University and used as received. The particle size was < 2 mm with an average moisture content of 10%. The bulk carbon (C), oxygen (O), hydrogen (H) and nitrogen (N) contents were 45.5 wt%, 47.7 wt%, 6.4 wt% and 0.4 wt%.

Biocrude Production. Red oak biocrude was produced with a commercially available spray-dried non-zeolitic alumina-based catalyst with nominal 70 micron particles in RTI's 1 ton per day CFP unit. The details about the unit and production of the CFP biocrudes have been previously reported.[5,9] The operating conditions of the CFP unit are given in Table 1.

Table 1. Operating conditions for the CFP unit for the production of the red oak biocrude.

Feed name	Red oak biocrude
Average mixing zone temperature	502°C
Average riser temperature	493°C
Average regenerator temperature	626°C
Average fluidization gas flow rate into mixing zone	463 scf/h
Average apparent vapor residence time in mixing zone	0.46 s
Average biomass feed rate	74 kg/h
Sampling point in CFP unit	Sample collected from hot coalescing filter

Hydrotreating Studies. A commercially available NiMo catalyst with high HDO activity and moderate hydrodesulfurization (HDS) activity was used for hydrotreating (TK-341, Haldor Topsoe A/S). The three hydrotreated biocrudes were obtained during a study of RTI's once-through down-flow trickle-bed hydrotreating pilot plant (Table 2).[5] This unit consist of two reactors in series with the reactor effluent separated in a high-pressure separator. The liquid effluent of the high-pressure separator is sent to a low-pressure separator and further stripped with nitrogen for removal of gases and non-condensed light hydrocarbons. The exit gases from the separators and the stripper are combined prior to sampling. Once-through pure hydrogen is used. The catalyst is diluted with an inert material (SiC mesh 60) in a 60/40 ratio. The catalyst was sulfided according to a procedure provided by Haldor Topsoe A/S with H_2S in H_2 (10 vol%) over 18 hours at 8 bar. The total flow of the gas mixture corresponded to 550 NL/h per litre of catalyst. It is important to note that the HDT oil was produced for co-processing analysis by blending different samples taken at different run-hours to achieve a targeted oxygen content. Therefore, this sample does not belong, per se, to a specific run-hour sample.

This journal is © The Royal Society of Chemistry 20xx

Table 2. Operating conditions for the hydrotreating pilot plant.

Feed name	Red oak biocrude
Time for stream hydrotreating (hours)	> 500
H_2 partial pressure (barg)	138
Average Temperature (°C)	300
LHSV (h^{-1})	0.33
H_2/oil ratio (Nl/l)	3300

Standard Analyses. Standard analyses of the biocrude and the hydrotreated products were conducted according to ASTM standard procedures listed in Table 3. Analyses were performed at Haldor Topsoe.

Table 3. Standard analyses of the biocrude and the hydrotreated products performed at Haldor Topsoe.

Analyses	Standard Method
S	ASTM D4294
H	ASTM D7171, D5291
C	ASTM D5291
O	Perkin Elmer 2400 Series II analyzer
Water Content	ASTM D4928
Ca, Fe, K, Mg, Na, P, Si	Custom methods based on ICP-MS and ICP-OES inspired by ASTM D5708
Simulated Distillation	ASTM D7213C
Micro-Conradson Residue	D4530

Silica Gel Fractionation. A silica gel fractionation was performed to obtain three fractions from each pyrolysis oil, consisting of the saturated and aromatic hydrocarbons, and polar compounds. Two grams of silica gel was dried overnight at 100 °C prior to column (10 mL disposable pipet) packing. After conditioning with 10 mL cyclohexane (HPLC grade, JT Baker, Phillipsburg NJ), approximately 20 mg of sample dissolved in 2 mL cyclohexane was loaded onto the column and allowed to equilibrate for 15 min. Saturated hydrocarbons were eluted in the first fraction with 20 mL of 100% cyclohexane. Next, 20 mL of a mixture of cyclohexane and dichloromethane (DCM) (90:10, v/v) eluted the aromatic hydrocarbons. In the third fraction, polar species were eluted with 10 mL of DCM:methanol (50:50, v/v) and 10 mL of methanol. All fractions were desolvated under N_2.

FT-ICR MS. Whole and fractionated bio-oil samples were dissolved to a concentration of 100 µg/mL in toluene (HPLC grade, JT Baker, Phillipsburg NJ) for positive-ion (+) atmospheric pressure photoionization (APPI) analysis. FT-ICR MS analysis was performed with a custom built 9.4 T FT-ICR mass spectrometer described elsewhere.[19,23–26] APPI ions were generated in a Thermo Scientific APPI source equipped with a krypton lamp that emits 10.0 and 10.6 eV photons, a nebulizer temperature of 300 °C, sheath gas of 60 p.s.i., auxiliary gas flow of ~4 L/min, and a sample flow rate of 50 µL/min. Fifty ~5 s time-domain transients were co-added for each spectrum. Mass resolving power at m/z 346 (center of distribution) was ~1,200,000 for the biocrude and ~1,300,000 at m/z 300 for the hydrotreated oil. Mass spectral calibration was performed with Predator software,[24] and formula assignments and class-specific DBE vs. carbon number imaging were conducted with PetroOrg© software.[27]

Results and Discussion

Bulk Analysis. Simulated distillation is commonly used in the petroleum industry for determination of boiling range distributions to give insight into the chemical composition of oils.[28] Simulated distillation method ASTM D7213 was developed for light and middle petroleum distillates, and its application to bio-oils should be done with understanding of its limitations. Biocrudes, specifically, are not compatible with simulated distillation due to thermal instability and incompatibility with GC-FID. The lower oxygen content of HDT samples, in principle, allows for better coverage of the simulated distillation, provided that all of the components boil below 600 °C. Despite its limitations, simulated distillation of bio-oils is useful for boiling range comparisons between samples. We therefore performed a simulated distillation for the biocrude and its hydrotreated counterpart (hydro) to estimate changes in boiling point and therefore carbon number with hydrotreatment (Figure 1). Hydro was found to have a higher maximum carbon number (C_{40} vs C_{34} for all compound classes) and higher wt% at the naphtha/middle distillate boundary (23 wt% vs 8 wt%) than the biocrude. These differences could be due to the removal of oxygen and cracking of high carbon number compounds; both of which are expected with hydrotreatment. Limitations of the simulated distillation are evident from the carbon number distributions (oxygen and hydrocarbon classes) derived from (+) APPI FT-ICR MS for the biocrude and hydro (Figure 2): maximum carbon number of C_{62} for hydro and C_{46} for biocrude.

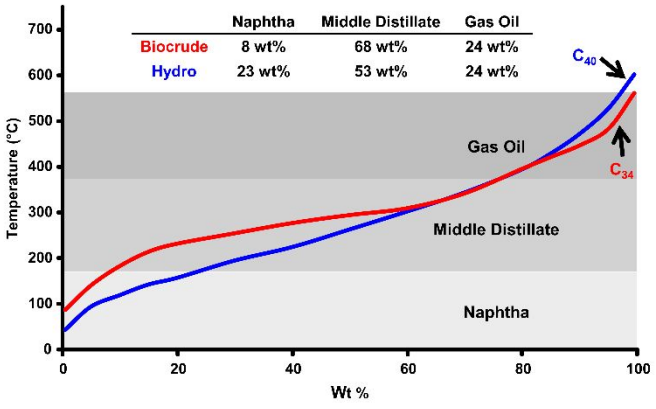

Figure 1. Simulated distillation of the oak biocrude and hydrotreated counterpart (hydro). Gravimetric results are shown for the naphtha, middle distillate, and gas oil regions. The carbon numbers at the end of the simulated distillation are shown at upper right.

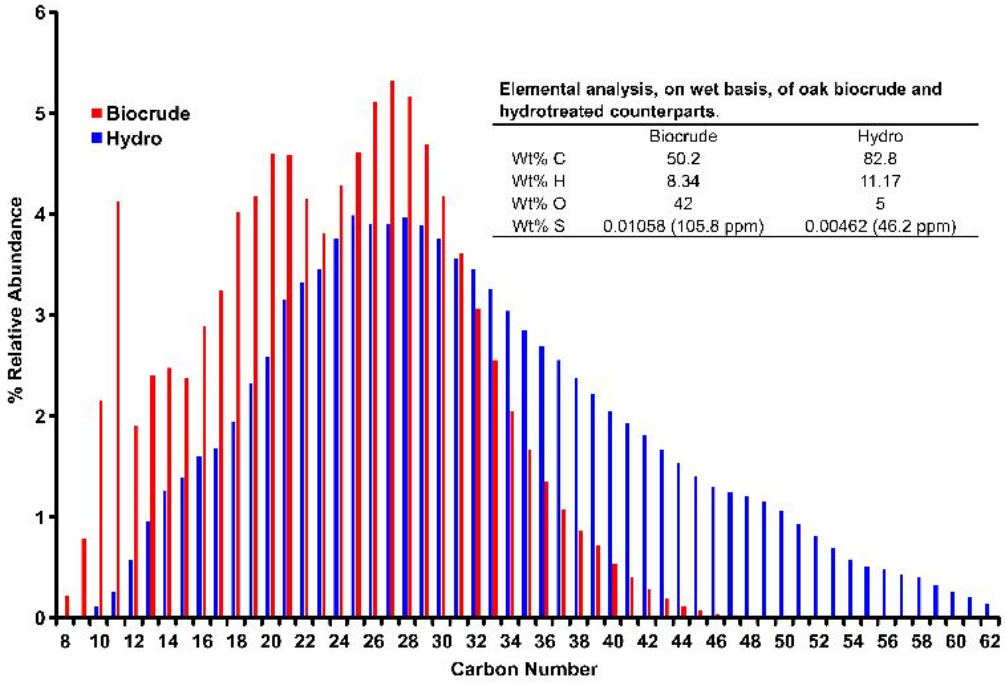

Figure 2. (+) APPI FT-ICR MS-derived carbon number distributions for all compound classes in oak biocrude and hydro.

It is well established that hydrotreatment of biocrude reduces the number of oxygen-containing compounds while increasing the wt% of carbon and hydrogen; supported by the elemental analysis (see inset table in Figure 2): e.g., oxygen content of 42 wt% for biocrude vs. 5% for its hydrotreated counterpart. Mass recoveries <100 wt% are due to loss of volatile species and incomplete combustion. Bulk analyses such as elemental analysis and simulated distillation give an abundance-weighted average of the sample components but do not provide the specific chemical compositions or structural information necessary for understanding bio-oil properties (see below).

Biocrude. (+) APPI FT-ICR MS of the oak biocrude yields a range of oxygen heteroatom classes between O_1 and O_{14} (Figure 3); as previously seen for other biocrudes.[18–21,29] The removal of oxygen species from this highly oxygenated biocrude is evident from the heteroatom class distribution: e.g., hydrocarbon class relative abundance of 17% for hydro, and greatly reduced relative abundance of O_4 – O_{14} oxygen classes. For hydro, the O_1 heteroatom class represents alcohol, ketone, ether, and/or aldehyde functionalities. In contrast, the low (<0.5%) hydrocarbon class relative abundance for

the biocrude reveals that the carbon measured by bulk analysis arises mainly from species that also contain oxygen atoms. The carbon number distributions for all species in the biocrude and hydro (Figure 2) show an increase in carbon number associated with hydrotreatment: i.e., an abundance-weighted average carbon number of 24 for the biocrude and 31 for hydro, indicating the formation of higher molecular weight compounds, most likely due

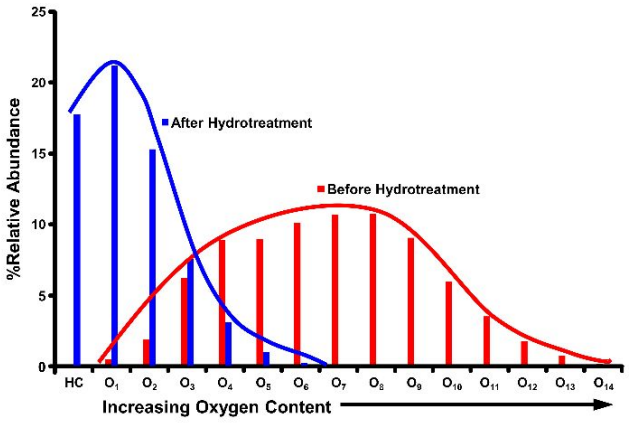

Figure 3. (+) APPI FT-ICR MS-derived heteroatom class distribution for oak biocrude and hydro.

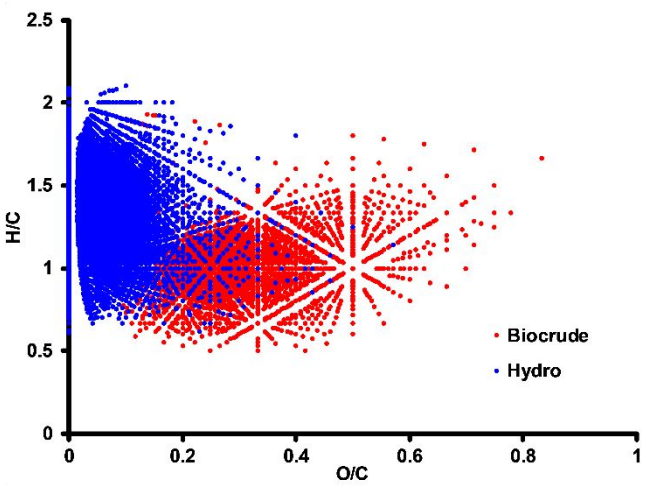

Figure 4. (+) APPI FT-ICR MS-derived van Krevelen plots for oak biocrude and hydro.

This journal is © The Royal Society of Chemistry 20xx

Please do not adjust margins

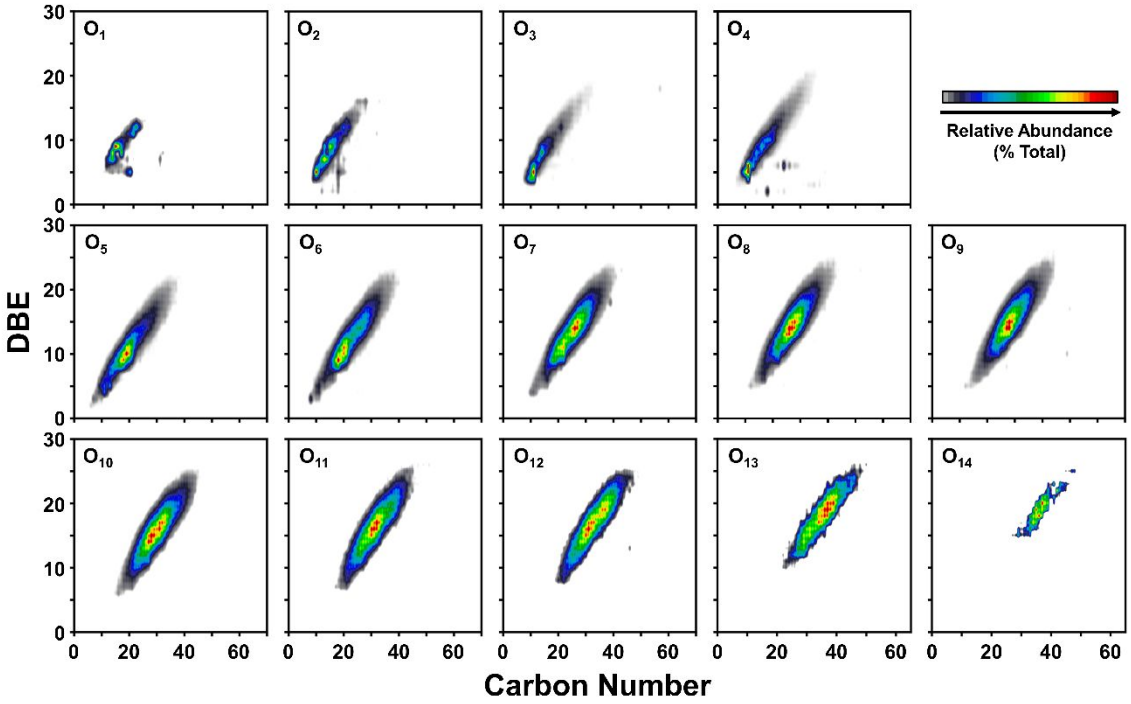

Figure 5. (+) APPI FT-ICR MS-derived isoabundance-contoured DBE vs carbon number plots for oxygen-containing heteroatom classes from oak biocrude.

to condensation and polymerization reactions. Polymerization is often reported for HDT reactions, and discussed in terms of higher molecular weight compound and coke formation.[7,30,31]

Positive APPI enables comparison of oxygen species from the biocrude and hydro through ionization of both polar and non-polar compounds. The (+) APPI-derived van Krevelen plots (Figure 4) indicate a shift to lower O/C ratio and higher H/C ratio upon hydrotreatment. The area spanned by hydro (O/C 0-0.3 and H/C 0.7-2.0) is similar to that for petroleum-like oils, whereas the biocrude does appear to fall within the usual range for lignin, cellulose, etc.[7,32] (+) APPI FT-ICR MS-derived DBE vs carbon number plots for the oxygen-containing classes from the biocrude follow the same trends in compositional space previously seen for other bio-oils (Figure 5).[6,7,18,21,29] These classes indicate condensed ring structures that increase in DBE and carbon number as the number of oxygen atoms increases. Moreover, the monotonic increase in DBE with increasing carbon number suggests linear polymers. The trends in compositional space do not reveal oxygen functionality, but do illustrate a wide range of compounds not seen by prior GC-MS analysis of CFP biocrudes.[2,3,5]

Hydrotreated Oils. The direct deoxygenation mechanism proposed by Mante et al.[9] for the present hydrotreating method is supported by the trends seen in the DBE vs carbon number plots for the O_1-O_5 heteroatom classes from hydro (Figure 6). The oxygen-containing species in hydro are presumably intermediates of the HDT mechanism. The wide compositional coverage that narrows as oxygen number increases indicates a primary mechanism of direct deoxygenation, because the species maintain aromaticity (DBE) at higher oxygen numbers. If the primary HDT mechanism were hydrogenation, then the oxygen intermediates would contain more hydrogen; hence lower DBE at higher oxygen numbers. As oxygen is removed, the compositional coverage shifts toward the final hydrocarbon compositional coverage (compare Figure 7, left to the O_1 heteroatom class in Figure 6). The species in this heteroatom

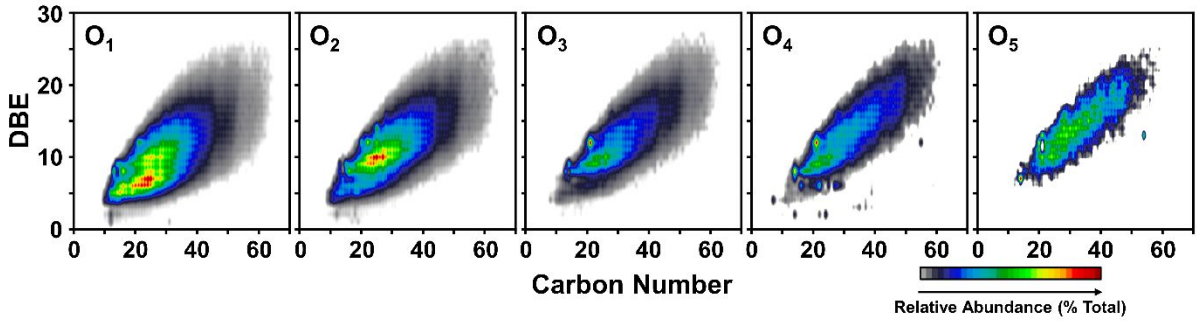

Figure 6. (+) APPI FT-ICR MS-derived isoabundance-contoured DBE vs carbon number plots for the O1-O5 heteroatom classes from hydro.

class represent the last intermediate, and therefore have the greatest degree of deoxygenation and hydrogenation of all the oxygen intermediates seen by (+) APPI FT-ICR MS.

An in-depth look at the hydrocarbons in hydro is provided by silica gel fractionation. As expected, silica gel gravimetric results (Table 4) show an increase in hydrocarbons and decrease in polar species on hydrotreatment. Mass recoveries less than 100 wt% are due to volatile species lost during desolvation. Prior to fractionation, the DBE vs. carbon number plot exhibits broad compositional coverage, without differentiation between the saturated and aromatic hydrocarbons. (Figure 7, left). Trend lines for the saturates and aromatic fractions were added to illustrate the structural trends in those fractions (Figure 7, middle and right). After fractionation, the DBE vs carbon number plots show that the saturated hydrocarbons have a very shallow slope (0.16) and narrow range of DBE (4-15) and carbon number (14-58), indicating a higher degree of saturation within the unit additions; such as alkanes and cycloalkanes. The aromatic hydrocarbons have a greater slope (0.25) and span a wider range of carbon number (14-65) and DBE (6-27) than the saturated hydrocarbons. Although aromatic rings appear to be present, polyaromatic hydrocarbons (PAHs) are not, illustrated by a slope less than the shallowest PAH slope (0.7).33 The lack of PAHs helps explain the low wt% of carbon residue in the hydrotreated sample (1.3 wt%) relative to the biocrude (22.1 wt%).

Table 4. Gravimetric results for the silica gel fractionation of oak biocrude and hydro.

	Biocrude (Wt%)	7
Saturated Hydrocarbons	2.67 ± 0.98	21.7 ± 2.31
Aromatic Hydrocarbons	2.43 ± 1.67	9.23 ± 1.66
Polars Species	90.8 ± 4.36	46.7 ± 3.26
Total	95.9	77.6

Conclusions

Positive APPI FT-ICR MS analysis showed a decrease in oxygen as well as increase in carbon number following hydrotreatment of an oak pyrolysis biocrude. The carbon number range was found to extend beyond what is accessible by simulated distillation, even for the more volatile hydro. A direct deoxygenation mechanism is supported by DBE vs carbon number plots, with aromaticity maintained for the oxygen-containing species after hydrotreatment. Silica gel fractionation separated saturated and aromatic hydrocarbons from hydro. The saturated hydrocarbons were found to contain cycloalkanes, whereas non-condensed aromatic hydrocarbons were seen in the aromatic fraction. The lack of PAHs accounts for the low amount of carbon residue from this oil. The molecular level information provided by high resolution mass spectrometry gives insight into chemical transformations that occur during hydrotreatment, as well as a better understanding of the properties of the hydrotreated oil. Further work is needed to identify oxygen functionalities.

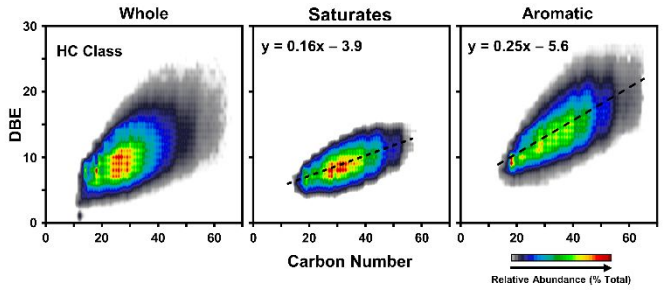

Figure 7. (+) APPI FT-ICR MS-derived isoabundance-contoured DBE vs carbon number plots for the hydrocarbons class from hydro and its silica gel saturated- and aromatic-hydrocarbon fractions. The abundance-weighted average carbon number for the saturated- and aromatic- hydrocarbons are shown.

Conflicts of interest

There are no conflicts to declare.

Acknowledgements

This work was supported by NSF Division of Chemistry through DMR-1157490 and DMR-1644779 and the State of Florida. We thank Greg T. Blakney, Donald F. Smith, and John P. Quinn for continued assistance in instrument maintenance and data analysis. The authors also thank Yuri E. Corilo for providing data processing and imaging software.

Notes and references

1 A. H. Zacher, M. V. Olarte, D. M. Santosa, D. C. Elliott and S. B. Jones, *Green Chem.*, 2014, **16**, 491–515.
2 V. Paasikallio, C. Lindfors, E. Kuoppala, Y. Solantausta, A. Oasmaa, J. Lehto and J. Lehtonen, *Green Chem.*, 2014, **16**, 3549–3559.
3 E. F. Iliopoulou, S. Stefanidis, K. Kalogiannis, A. C. Psarras, A. Delimitis, K. S. Triantafyllidis and A. A. Lappas, *Green Chem.*, 2014, **16**, 662–674.
4 R. H. Venderbosch, *ChemSusChem*, 2015, **8**, 1306–1316.
5 D. C. Dayton, J. R. Carpenter, A. Kataria, J. E. Peters, D. Barbee, O. D. Mante and R. Gupta, *Green Chem.*, 2015, **17**, 4680–4689.
6 R. L. Ware, S. M. Rowland, R. P. Rodgers and A. G. Marshall, *Energy & Fuels*, 2017, **31**, 8210–8216.
7 D. J. McClelland, A. H. Motagamwala, Y. Li, M. R. Rover, A. M. Wittrig, C. Wu, J. S. Buchanan, R. C. Brown, J. Ralph, J. A. Dumesic and G. W. Huber, *Green Chem.*, 2017, **19**, 1378–1389.
8 A. Croce, E. Battistel, S. Chiaberge, S. Spera, F. De Angelis and S. Reale, *ChemSusChem*, 2017, **10**, 171–181.
9 O. D. Mante, D. C. Dayton, J. Gabrielsen, N. L. Ammitzboll, D. Barbee, S. Verdier and K. Wang, *Green Chem.*, 2016, **18**, 6123–6135.
10 M. V. Olarte, A. H. Zacher, A. B. Padmaperuma, S. D. Burton, H. M. Job, T. L. Lemmon, M. S. Swita, L. J. Rotness, G. N. Neuenschwander, J. G. Frye and D. C. Elliott, *Top. Catal.*, 2016, **59**, 55–64.
11 A. H. Zacher, D. C. Elliott, M. V. Olarte, D. M. Santosa, F. Preto and K. Iisa, *Energy and Fuels*, 2014, **28**, 7510–7516.

This journal is © The Royal Society of Chemistry 20xx

Please do not adjust margins

12 N. Schwaiger, D. C. Elliott, J. Ritzberger, H. Wang, P. Pucher and M. Siebenhofer, *Green Chem.*, 2015, **17**, 2487–2494.
13 D. C. Elliott, H. Wang, M. Rover, L. Whitmer, R. Smith and R. Brown, *ACS Sustain. Chem. Eng.*, 2015, **3**, 892–902.
14 D. C. Elliott, H. Wang, R. French, S. Deutch and K. Iisa, *Energy and Fuels*, 2014, **28**, 5909–5917.
15 D. C. Elliott, T. R. Hart, G. G. Neuenschwander, L. J. Rotness, M. V. Olarte, A. H. Zacher and Y. Solantausta, *Energy and Fuels*, 2012, **26**, 3891–3896.
16 A. R. Ardiyanti, A. Gutierrez, M. L. Honkela, A. O. I. Krause and H. J. Heeres, *Appl. Catal. A Gen.*, 2011, **407**, 56–66.
17 F. A. Agblevor, D. C. Elliott, D. M. Santosa, M. V. Olarte, S. D. Burton, M. Swita, S. H. Beis, K. Christian and B. Sargent, *Energy and Fuels*, 2016, **30**, 7947–7958.
18 E. A. Smith, S. Park, A. T. Klein and Y. J. Lee, *Energy & Fuels*, 2012, **26**, 3796–3802.
19 J. M. Jarvis, D. S. Page-dumroese, N. M. Anderson, Y. Corilo and R. P. Rodgers, *Energy & Fuels*, 2014, **28**, 6438–6446.
20 E. A. Smith, C. Thompson and Y. J. Lee, *Bull. Korean Chem. Soc.*, 2014, **35**, 811–814.
21 Y. Liu, Q. Shi, Y. Zhang, Y. He, K. H. Chung, S. Zhao and C. Xu, *Energy & Fuels*, 2012, **26**, 4532–4539.
22 J. Hertzog, V. Carré, Y. Le Brech, C. L. Mackay, A. Dufour, O. Mašek and F. Aubriet, *Anal. Chim. Acta*, 2017, **969**, 26–34.
23 N. K. Kaiser, J. P. Quinn, G. T. Blakney, C. L. Hendrickson and A. G. Marshall, *J. Am. Soc. Mass Spectrom.*, 2011, **22**, 1343–1351.
24 G. T. Blakney, C. L. Hendrickson and A. G. Marshall, *Int. J. Mass Spectrom.*, 2011, **306**, 246–252.
25 A. G. Marshall, C. L. Hendrickson and G. S. Jackson, *Mass Spectrom. Rev.*, 1998, **17**, 1–35.
26 F. Xian, C. L. Hendrickson, G. T. Blakney, S. C. Beu and A. G. Marshall, *Anal. Chem.*, 2010, **82**, 8807–8812.
27 © PetroOrg, 2017.
28 M. M. Boduszynski, *Energy & Fuels*, 1987, **1**, 2–11.
29 J. M. Jarvis, A. M. McKenna, R. N. Hilten, K. C. Das, R. P. Rodgers and A. G. Marshall, *Energy and Fuels*, 2012, **26**, 3810–3815.
30 D. C. Elliott, T. R. Hart, G. G. Neuenschwander, L. J. Rotness and A. H. Zacher, *Environ. Prog. Sustain. Energy*, 2009, **28**, 442–449.
31 H. Wang, J. Male and Y. Wang, *ACS Catal.*, 2013, **3**, 1047–1070.
32 I. Miettinen, S. Kuittinen, V. Paasikallio, M. Mäkinen, A. Pappinen and J. Jänis, *Fuel*, 2017, **207**, 189–197.

Table of Contents Graphic

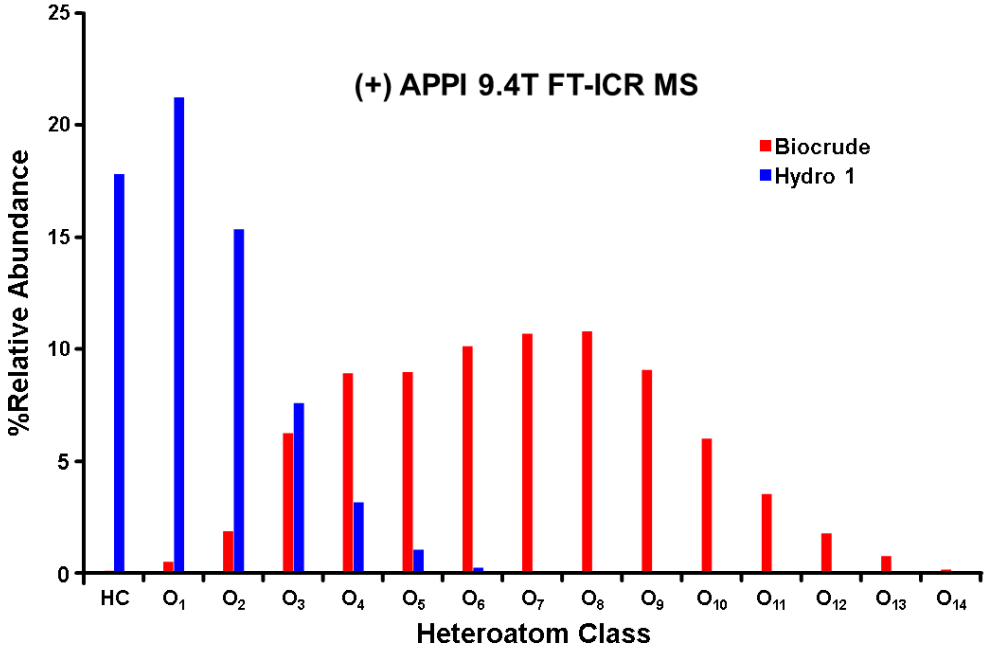

279x215mm (96 x 96 DPI)